Robust Navigation for Urban Air Mobility via Tight Coupling of GNSS with Terrestrial Radionavigation and Inertial Sensing

Robert Tenny*, Todd E. Humphreys†
*Department of Electrical and Computer Engineering, The University of Texas at Austin
†Department of Aerospace Engineering and Engineering Mechanics, The University of Texas at Austin

BIOGRAPHIES

Robert Tenny (BS, Electrical Engineering, University of Kansas) is a graduate student in the department of Electrical and Computer Engineering at The University of Texas at Austin, and a member of the UT Radionavigation Laboratory. His research interests include GNSS signal processing, sensor fusion, and software-defined radio.

Todd Humphreys (BS, MS, Electrical Engineering, Utah State University; PhD, Aerospace Engineering, Cornell University) is a professor in the department of Aerospace Engineering and Engineering Mechanics at The University of Texas at Austin, where he directs the Radionavigation Laboratory. He specializes in the application of optimal detection and estimation techniques to problems in secure, collaborative, and high-integrity perception, with an emphasis on navigation, collision avoidance, and precise timing. His awards include The University of Texas Regents' Outstanding Teaching Award (2012), the National Science Foundation CAREER Award (2015), the Institute of Navigation Thurlow Award (2015), the Qualcomm Innovation Fellowship (2017), the Walter Fried Award (2012, 2018), and the Presidential Early Career Award for Scientists and Engineers (PECASE, 2019). He is a Fellow of the Institute of Navigation and of the Royal Institute of Navigation.

ABSTRACT

This paper presents a method of tightly coupling carrier-phase-differential GNSS (CDGNSS) with terrestrial radionavigation system (TRNS) signals and data to build a robust positioning, velocity, and timing (PVT) solution for urban air mobility (UAM). UAM will require precise and robust PVT solutions that are resilient to interference and jamming. CDGNSS offers absolute positioning with high availability and sub-decimeter accuracy but cannot serve as the sole source of PVT for UAM because of its vulnerability to interference: a single potent GNSS jammer could deny UAM service across an entire city were GNSS the sole means UAM navigation. TRNS signals are stronger than those of GNSS and offer additional frequency diversity. Their multipath errors, although larger than for GNSS at street level due to the low elevation angles with which TRNS signals propagate from terrestrial transmitters, are manageably small at altitudes where UAM vehicles will operate. Thus, TRNS offers an attractive backup to GNSS for UAM. This paper explores two techniques for fusion of TRNS and CDGNSS: loosely- and tightly-coupled. The loosely-coupled technique fuses information from the two sensing modalities at the level of full PVT solutions. The tightly-coupled technique explored here fuses GNSS carrier phase and pseudorange measurements with TRNS pseudorange and calibrated pressure sensor measurements, together with inertial sensor measurements, to produce a unified PVT solution. Innovations-based measurement exclusion is applied to reduce the impact of GNSS and TRNS multipath errors and of pressure anomalies due, e.g., to ground effect at take-off and landing. Both loosely- and tightly-coupled techniques are tested on an aerial vehicle platform in an environment where both GNSS and TRNS signals are available. Error growth of the tightly-coupled technique during extended intervals of GNSS denial is studied to determine whether UAM service could continue uninterrupted when only inertial and TRNS measurements remain available.

INTRODUCTION

Central to the transportation revolution that will be driven by urban air mobility (UAM) is the problem of robust and secure navigation. Urban environments offer more challenges, such as interference and multipath, when compared to open-sky conditions. As the only positioning system that offers absolutely-referenced meter-level accuracy with global coverage,

GNSS will no doubt play a significant role in this revolution. If strengthened against jamming and spoofing, carrier-phase-differential GNSS (CDGNSS), coupled with low-cost inertial sensing, will be nearly sufficient for position, velocity, and timing (PVT) needs. But nearly sufficient is insufficient: it is not enough for a UAM PVT solution to offer decimeter-accurate positioning with 99% availability, or even 99.9% availability. UAM will demand that its navigation systems offer dm-accurate positioning with integrity risk on the order of 10^{-7} for a meter-level alert limit and availability with several more 9s than 99.9% [1]–[4].

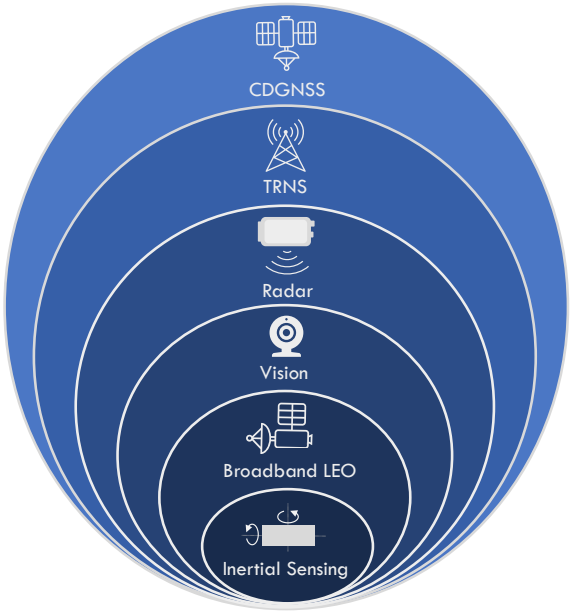

Fig. 1: Diagram of deep layered navigation. Overlapping layers of navigation to provide a PVT solution with high availability even when some of the layers are not available.

This paper's technique is best viewed as one part of a comprehensive navigation solution concept called deep-layered navigation (DLN) in which synergistic but independent navigation systems are layered to increase accuracy and robustness (1). DLN is the navigation analog of the "defense in depth" concept in information security, where multiple layers of security controls and checkpoints are emplaced throughout a system such that even when some layers are breached, security is maintained. Likewise, in the safety-of-life UAM navigation context, multiple layers of navigation systems, all interoperable and mutually-reinforcing but substantially independent, are an essential defense against the whims of Mother Nature and the foibles of human nature.

At DLN's core sits redundant inertial navigation, which is virtually impervious to radio frequency (RF) interference, poor weather, signal blockage, and data ambiguity. The outermost layer—the default navigation system and first line of defense—is a specialized variant of inertially-aided CDGNSS, recently developed in [5], [6], that has been substantially secured against spoofing and substantially hardened against the multipath and signal blockage conditions of the urban *ground vehicle* environment, which can be considered a worst-case realization of the urban air vehicle environment. But despite its coupling with inertial sensing, the technique developed in [5] cannot tolerate extended GNSS outages. A secondary source of absolute PVT is required to bound the growth of position errors.

TRNS is the second line of defense in this paper's DLN concept, and the primary focus of the paper. Its pseudorange measurements to surrounding beacons are independent of, but fully interchangeable with, GNSS measurements. TRNS beacons provide much stronger signals compared to GNSS, operate at a different frequency, and offer a full absolutely-referenced backup PVT solution to GNSS. In particular, this paper explores tight coupling with NextNav's Metropolitan Beacon System (MBS). MBS is particularly attractive for UAM because its signals carry not only wideband (multipath-resistant) synchronization sequences for ranging but also corrections data for barometric altitude determination and, for CDGNSS.

This paper's development of a tightly-coupled GNSS-TRNS-inertial PNT system is a prelude to upcoming work on comprehensive deep-layered navigation for UAM, including additional layers based on radar localization, visual odometry, and

LEO-satellite-provided GNSS.

Related Work

Augmentation of GNSS with terrestrial signals has been explored and shown to provide an added benefit over exclusive use of GNSS [7], [8]. But these techniques were demonstrated only on ground vehicles, and the sensor integration with CDGNSS was not tightly-coupled: the terrestrial signals were not incorporated in a way that permitted aiding of the ambiguity resolution process critical to CDGNSS. Loose coupling between GNSS and TRNS has been used to augment GNSS and provide an increase in both accuracy and availability on aerial vehicles [9]–[11]. But these methods fuse standard GNSS, not CDGNSS, with TRNS, and thus lack the decimeter accuracy that will be desirable, if not required, for UAM. Relative ranging measurements from ultra wide band (UWB) systems have been used to constrain integer ambiguities in CDGNSS and improve accuracy even with degraded GNSS reception [12]. Although UWB systems provide adequate performance, the limited range of the UWB signal makes it an unfavorable choice for UAM. Fusion of GNSS and signals of opportunity has been explored for aerial vehicles with promising results [13], [14]. But for a safety-of-life application like UAM, it is likely that signals of opportunity will be viewed less favorably than a dedicated TRNS as a secondary means of navigation.

Contributions

This paper makes four primary contributions. First, it presents and demonstrates the first use of tightly-coupled CDGNSS, TRNS, and inertial sensing to provide a secure and robust PVT solution. Second, it develops a novel innovations-based measurement exclusion technique which mitigates the impact of GNSS and TRNS multipath errors and pressure anomalies. Third, it offers a comparative analysis of loose and tight coupling on an aerial vehicle in an environment where only TRNS signals are available. Fourth, this paper preforms a study of error growths during periods of GNSS denial to determine whether PVT requirements for UAM could be met despite extended intervals of GNSS denial.

MEASUREMENT MODELS

This section presents the TRNS measurement models for the tightly- and loosely-coupled estimation strategies. In the loosely-coupled case, the TRNS measurement is the position determined by the TRNS receiver. In the tightly-coupled case, the TRNS measurements are pseudorange and altitude derived from barometric pressure. The measurements are fused with inertial sensing data and GNSS position and attitude solutions (loosely-coupled) or raw GNSS observables (tightly-coupled). Models for the inertial and GNSS measurements may be found in [5] and [16].

Loose Coupling

The position measurement $\mathbf{z}_{\mathrm{lc}}(k)$ at time k from the TRNS receiver is modeled as containing the true position $\mathbf{x}_{\mathrm{lc}}(k)$, a bias from the true position $\mathbf{b}_{\mathrm{lc}}(k)$, and white Gaussian measurement noise $\mathbf{w}_{\mathrm{lc}}(k)$:

$$\mathbf{z}_{\mathrm{lc}}(k) = \mathbf{x}_{\mathrm{lc}}(k) + \mathbf{b}_{\mathrm{lc}}(k) + \mathbf{w}_{\mathrm{lc}}(k) \tag{1}$$

The position bias $\mathbf{b}_{\mathrm{lc}}(k)$ is modeled as a mean-reverting Ornstein–Uhlenbeck (OU) process with white Gaussian noise $\mathbf{v}_{\mathrm{lc}}(k)$:

$$\mathbf{b}_{\mathrm{lc}}(k+1) = \alpha_{\mathrm{lc}}\mathbf{b}_{\mathrm{lc}}(k) + \mathbf{v}_{\mathrm{lc}}(k) \tag{2}$$

The term α_{lc} determines how quickly the process reverts back to zero. The mean reversion is governed by the time step $T(k) = t_{k+1} - t_k$ and the time constant τ_{lc} of the exponential decay:

$$\alpha_{\mathrm{lc}} = e^{-T(k)/\tau_{\mathrm{lc}}} \tag{3}$$

Tight Coupling

The TRNS measurements utilized for tight coupling are the TRNS pseudoranges and barometric-pressure-based altitude measurements. The TRNS pseudorange to transmitter i at time k, is modeled as including the true range to the TRNS transmitter $\rho_i(k)$, the receiver clock offset between the receiver clock and GPS time $\delta t_{\mathrm{rx}}(k)$, the transmitter clock offset $\delta t_i(k)$, multipath error $m_i(k)$, and white Gaussian measurement noise $w_i(k)$:

$$P_i(k) = \rho_i(k) + [\delta t_{\mathrm{rx}}(k) - \delta t_i(k)]c + m_i(k) + w_i(k) \tag{4}$$

The receiver clock is modeled as a temperature-compensated crystal oscillator (TCXO) with the two-parameter clock model given in [15]. The receiver clock offset $\delta t_{\mathrm{rx}}(k)$ evolves in time based on the clock offset rate $\dot{\delta} t_{\mathrm{rx}}(k)$, time step $T(k)$, and noise $\boldsymbol{v}(k)$:

$$\begin{bmatrix} \delta t_{\mathrm{rx}}(k+1) \\ \dot{\delta} t_{\mathrm{rx}}(k+1) \end{bmatrix} = \begin{bmatrix} 1 & T(k) \\ 0 & 1 \end{bmatrix} \begin{bmatrix} \delta t_{\mathrm{rx}}(k) \\ \dot{\delta} t_{\mathrm{rx}}(k) \end{bmatrix} + \begin{bmatrix} v_1(k) \\ v_2(k) \end{bmatrix} \tag{5}$$

$$\boldsymbol{v}(k) = \begin{bmatrix} v_1(k) \\ v_2(k) \end{bmatrix} \tag{6}$$

The receiver clock offset noise $\boldsymbol{v}(k)$ is assumed to be zero mean with a variance that is a function of two parameters, h_0 and h_{-2}, related to the asymptotes of the Allan variance of the receiver clock [15]:

$$\mathbb{E}\left[\boldsymbol{v}(k)\boldsymbol{v}^{\mathsf{T}}(k)\right] = S_{\mathrm{g}} \begin{bmatrix} \frac{T^3(k)}{3} & \frac{T^2(k)}{2} \\ \frac{T^2(k)}{2} & T(k) \end{bmatrix} + S_{\mathrm{f}} \begin{bmatrix} T(k) & 0 \\ 0 & 0 \end{bmatrix} \tag{7}$$

$$S_{\mathrm{g}} = 2\pi^2 h_{-2} \tag{8}$$

$$S_{\mathrm{f}} = \frac{h_0}{2} \tag{9}$$

The TRNS transmitter clocks are disciplined by a GNSS receiver to keep them close to GPS time, but a small offset remains. The offset between the ith transmitter's clock and GPS time, $\delta t_i(k)$, is modeled as a mean-reverting OU processes with α_{tx} being modeled as in (3) but having a unique time constant τ_{tx} to match the behavior of the transmitter clock offsets.

$$\delta t_i(k+1) = \alpha_{\mathrm{tx}} \delta t_i(k) + v_i(k) \tag{10}$$

$$\alpha_{\mathrm{tx}} = e^{-T(k)/\tau_{\mathrm{tx}}} \tag{11}$$

The TRNS receiver measures altitude using a barometric pressure sensor that is calibrated over the NextNav MBS network using information from NextNav's weather stations. The calibration does not occur continuously; rather, it is only updated once per day. The long update interval allows for pressure biases to accumulate due to short-term changes in temperature, pressure, or other changes in weather. The altitude measurement at time k, $z_{\mathrm{p}}(k)$, is modeled as containing the true altitude $x_{\mathrm{p}}(k)$, a bias $b_{\mathrm{p}}(k)$, and white Gaussian measurement noise $w_{\mathrm{p}}(k)$:

$$z_{\mathrm{p}}(k) = x_{\mathrm{p}}(k) + b_{\mathrm{p}} + w_{\mathrm{p}}(k) \tag{12}$$

The measurement bias is modeled as an OU process with white Gaussian noise $v_{\mathrm{p}}(k)$ and with α_{p} is modeled according to (3) with a unique time constant τ_{p} that is selected to model the pressure sensor errors:

$$b_{\mathrm{p}}(k+1) = \alpha_{\mathrm{p}} b_{\mathrm{p}}(k) + v_{\mathrm{p}}(k) \tag{13}$$

$$\alpha_{\mathrm{p}} = e^{-T(k)/\tau_{\mathrm{p}}} \tag{14}$$

ESTIMATOR

This paper incorporates the measurement models of the TRNS measurements into the Radionavigation Laboratory's (RNL) precise positioning engine, called PpEngine [5], [16], [17]. The positioning engine was constructed in two versions. The first version loosely couples the GNSS and TRNS measurements with the inertial sensor measurements (Fig. 2). The second tightly couples the GNSS and TRNS measurements with the inertial sensor measurements (Fig. 2).

It will be convenient to define the following reference frames:

u: The *IMU frame* is centered at and aligned with the IMU accelerometer triad.

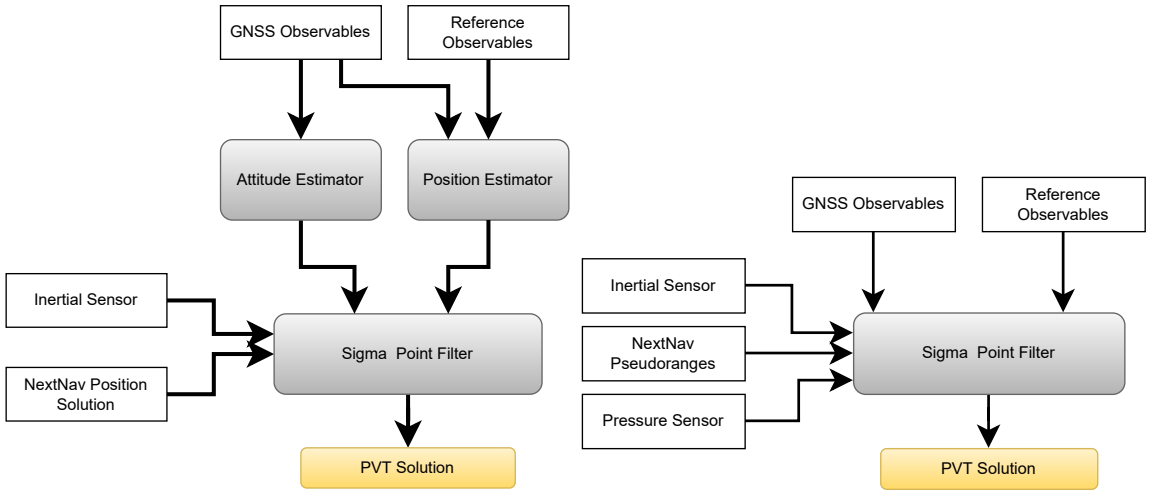

Fig. 2: Left: In the loosely-coupled configuration, the GNSS-based position attitude estimates are fused with inertial data and the TRNS-based position estimate to produce a PVT solution. Right: In the tightly-coupled configuration, raw measurements from each source are combined in a single estimator to produce a PVT solution.

b: The *body frame* has its origin at the phase center of the aerial test vehicle's primary GNSS antenna. Its x axis points towards the phase center of the secondary antenna, its y axis is aligned with the boresight vector of the primary antenna, and its z axis completes the right-handed triad.

w: The *world frame* is a fixed geographic East-North-Up (ENU) frame, with its origin at the phase center of the reference GNSS antenna, which is located at a fixed base station with known coordinates.

Both the loosely- and tightly-coupled estimator states are an augmented version of the original PpEngine state containing the aerial vehicle's position in the world frame $\mathbf{r}_k^{\mathrm{w}}$, velocity in the world frame $\mathbf{v}_k^{\mathrm{w}}$, attitude expressed as Euler error angles between the body frame and the world frame $\mathbf{e}$, accelerometer bias in the IMU frame $\mathbf{b}_{\mathrm{a}}^{\mathrm{u}}$, and gyro bias in the IMU frame $\mathbf{b}_{\mathrm{g}}^{\mathrm{u}}$:

$$\mathbf{X} = \left\{\mathbf{r}_k^{\mathrm{w}}, \mathbf{v}_k^{\mathrm{w}}, \mathbf{e}, \mathbf{b}_{\mathrm{a}}^{\mathrm{u}}, \mathbf{b}_{\mathrm{g}}^{\mathrm{u}}\right\} \tag{15}$$

Loosely-Coupled Estimator

The loosely-coupled implementation of PpEngine determines the aerial vehicle's state (16) by cascading multiple estimators (Fig. 2). The CDGNSS position of the primary GNSS antenna is determined using the double differenced pseudoranges and carrier phase measurements from the aerial vehicle's primary GNSS antenna and the reference receiver [17]. A separate position measurement is determined by the NextNav TRNS receiver, and its fixed position relative to the phase center of the aerial vehicle's primary GNSS antenna. Next, the two dimensional attitude of the aerial vehicle is estimated using the double differenced pseudoranges and carrier phase measurements between the two GNSS antennas and the known baseline between the antennas [17]. In addition, a position and attitude estimate is determine using the measurements from the inertial sensor. These separate position and attitude solutions and their estimated covariance are cascaded into a second level estimator to produce the complete position and attitude solution (16) with the state augmented to include the TRNS position bias $\mathbf{b}_0^{\mathrm{w}}$.

$$\mathbf{X}_{\mathrm{lc}} = \left\{\mathbf{r}_k^{\mathrm{w}}, \mathbf{v}_k^{\mathrm{w}}, \mathbf{e}, \mathbf{b}_{\mathrm{a}}^{\mathrm{u}}, \mathbf{b}_{\mathrm{g}}^{\mathrm{u}}, \mathbf{b}_{\mathrm{lc}}^{\mathrm{w}}\right\} \tag{16}$$

Tightly-Coupled Estimator

The tightly-coupled version of PpEngine incorporates all the sensor measurements directly into a single estimator (Fig. 2). The single estimator is used to determine the state [5], [18]. The estimator state (17) was augmented by including estimates of the TRNS receiver clock offset δt_{rx}, TRNS receiver clock offset rate $\dot{\delta t}_{\mathrm{rx}}$, transmitter clock offsets for n of transmitters $\delta t_i, \ldots, \delta t_n$, and pressure sensor offset $b_{\mathrm{p}}^{\mathrm{w}}$.

$$\mathbf{X}_{\mathrm{tc}} = \left\{ \mathbf{r}_k^{\mathrm{w}}, \mathbf{v}_k^{\mathrm{w}}, \mathbf{e}, \mathbf{b}_{\mathrm{a}}, \mathbf{b}_{\mathrm{g}}, \delta t_{\mathrm{rx}}, \dot{\delta t}_{\mathrm{rx}}, \delta t_1, \ldots, \delta t_n, b_{\mathrm{p}}^{\mathrm{w}} \right\} \tag{17}$$

Estimating the clock parameters for both the local clock and transmitter clock from the pseudorange measurements is not fully observable. However, the local clock offset can be separated from the transmitter clock offsets stylistically. The errors that are constant across all transmitters will show up in the local clock offset. Any errors that are unique to one transmitter will appear in the clock offset of that transmitter.

The transmitter clock offsets are being estimated despite not being fully observable, because the addition of a second TRNS receiver would allow for the transmitter clock offset to be observable. If two UAM vehicles each had their own TRNS receiver the vehicles would be able to jointly estimate the TRNS transmitter clock parameters. This would make the TRNS transmitter clock offsets observable for any UAM network operating two or more vehicles.

Innovations Testing

The tightly-coupled PpEngine preforms outlier exclusion to reject TRNS measurements that may be affected by multipath, and pressure measurements anomalies. The outliers are detected by preforming a hypothesis test on the TRNS pseudorange innovations, and the pressure sensor innovations. The normalized innovation squared (NIS) (18) at time k is found by normalizing the innovation $\boldsymbol{\nu}(k)$ with the innovation covariance $\mathbf{S}(k)$.

$$\mathrm{NIS} = \boldsymbol{\nu}^{\mathsf{T}}(\mathrm{k})\mathbf{S}^{-1}(\mathrm{k})\boldsymbol{\nu}(\mathrm{k}) \tag{18}$$

The NIS is distributed as Chi squared with nz degrees of freedom, where nz is the number of measurements at epoch k. The NIS can be used as a test statistic in a hypothesis test with $\nu > 0$ is the threshold that yields the chosen probability of false alarm P_F.

$$\mathrm{NIS} \underset{\mathrm{H_0}}{\overset{\mathrm{H_1}}{\gtrless}} \nu^* \tag{19}$$

An outlier is detected when the NIS surpasses the threshold value ν^*. Further processing then identifies and excludes the outlier measurement from the update.

DATA COLLECTION

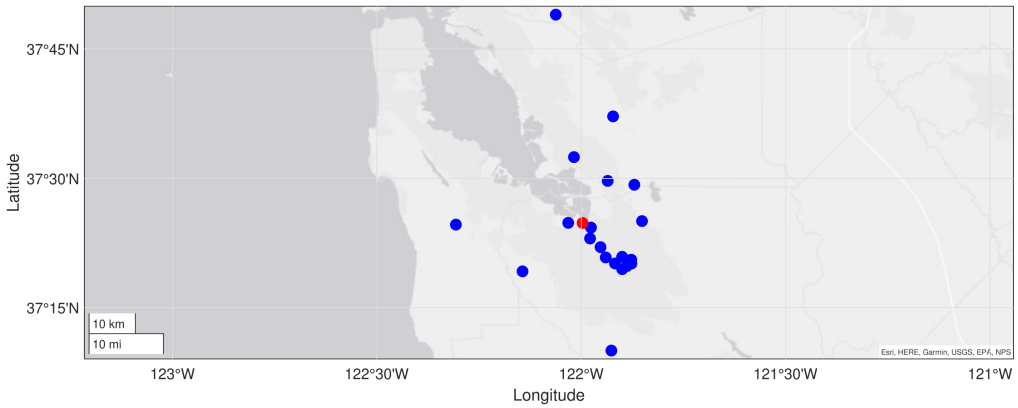

Fig. 3: Map of the location of the TRNS transmitters visible to the TRNS receiver during flight and the flight location in red

A data set was collected using the UT RNL aerial test vehicle (Fig. 5). The aerial test vehicle is a DJI Matrice 300 multi-rotor vehicle with a sensors mounted on the vehicle. The sensors used in this data set are a dual antenna GNSS L1

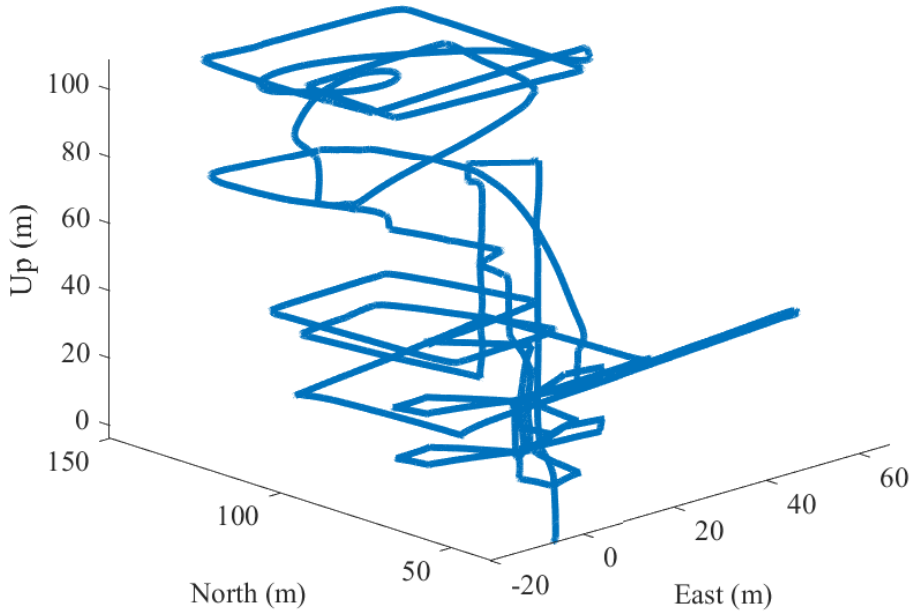

Fig. 4: Flight path of the aerial vehicle during data collection flight. The position is shown in meters from the phase center of the reference receiver antenna in the ENU frame.

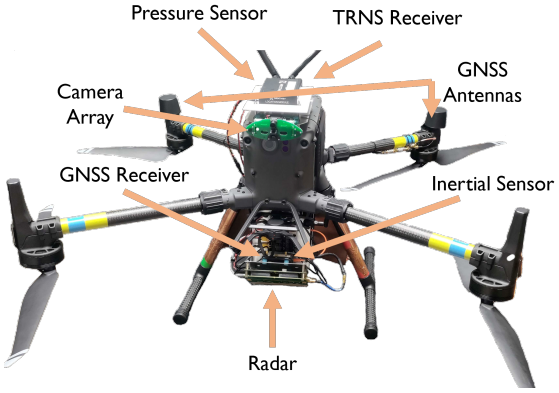

Fig. 5: RNL's aerial test vehicle. It carries two single frequency GNSS antennas, a radar sensor, TRNS receiver, pressure sensor, and three cameras.

receiver, a NextNav TRNS receiver, and a Bosch BMX055 consumer grade inertial measurement unit (IMU). In addition, a GNSS reference receiver was placed near the planned flight location. The dataset contains dual antenna GNSS L1 double differenced pseudoranges, carrier phase measurements, TRNS position solution, TRNS pseudoranges, calibrated barometric pressure sensor measurements, and inertial sensor measurements. The reference and aerial test vehicle GNSS receivers utilized the RNL's *RadioLynx*, GNSS front end with a 5 MHz bandwidth, and was processed with the PpRx software-defined GNSS receiver [16], [19]–[22].

A data collection flight was preformed in an area where NextNav TRNS signals are available (Fig. 3). The flight path was limited to 80 meters by 100 meters in the east and north directions due to constraints on communication range with the aerial vehicle. FAA regulations limited the altitude ceiling to 121 meters above ground level. The full flight path shown in (Fig.

4). The recorded dataset includes approximately 900 seconds of data at different altitudes and varying vehicle velocities.

RESULTS

The following section presents an analysis of the TRNS pseudoranges and an evaluation of the loosely- and tightly-coupled implementations of the position estimator.

Analysis of TRNS Pseudoranges

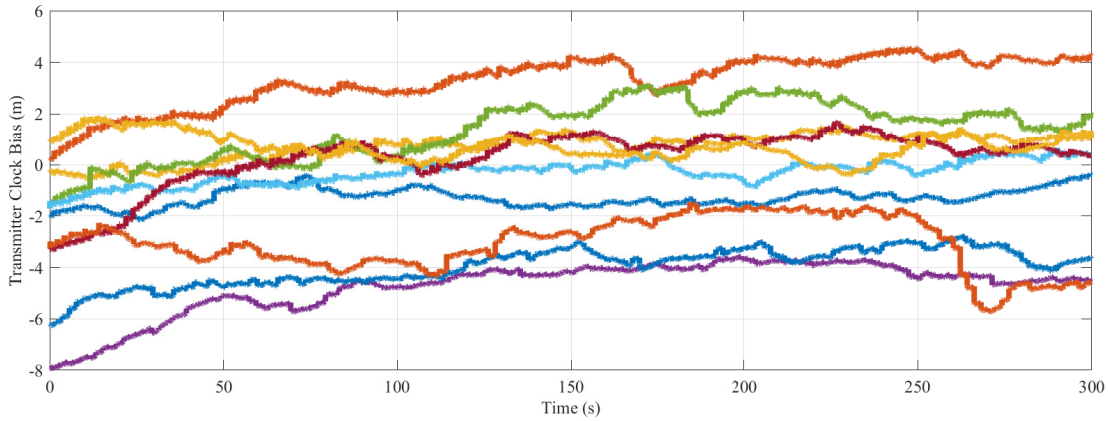

Fig. 6: Estimated TRNS transmitter clock offset of the TRNS transmitters in meters

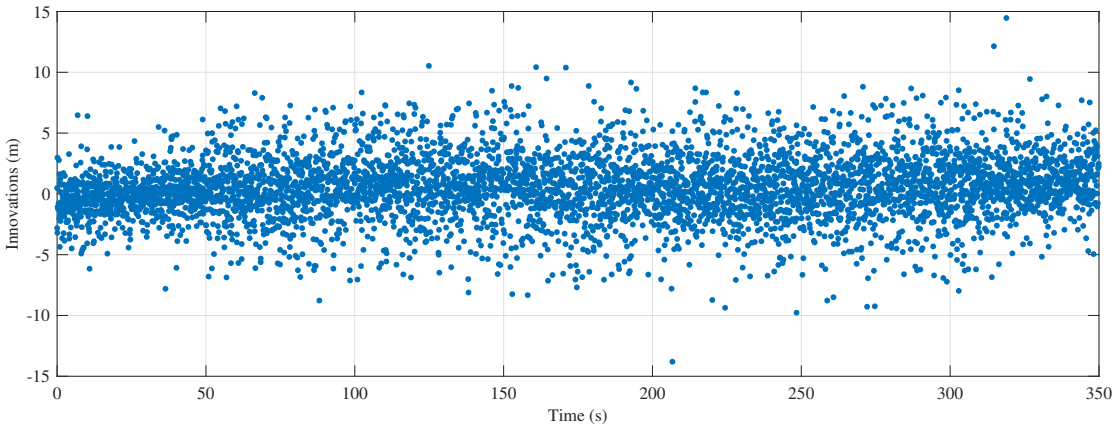

Fig. 7: TRNS pseudorange innovations in meters

The TRNS pseudoranges were analyzed using the collected dataset and the tightly-coupled version of PpEngine. The estimated TRNS transmitter clock offsets (Fig. 6) were observed to determine the behavior of the TRNS transmitter clocks. The estimated transmitter clock offsets were found to be non zero and unique to each transmitter. The largest difference between transmitter clock offsets indicates that the transmitter clocks differ by as much as 30 nanoseconds. These estimated TRNS transmitter clock offsets are not fully observable meaning part of the estimate may be due to the TRNS receiver clock offset.

The TRNS pseudorange innovations (Fig. 7) were examined and found to be nearly zero-mean and white, demonstrating that the pseudorange errors were well modeled. This shows that despite the lack of full observability of the clock offsets, the location of the TRNS receiver can still be estimated.

Artificial GNSS Outage

A long scale GNSS outage experiment was preformed to represent a worst case scenario of a full loss of GNSS availability. The experiment was preformed for both loosely- and tightly-coupled estimators. The loosely-coupled solution (Fig. 8) shows that during a long duration GNSS outage a bias between the CDGNSS position and TRNS position arises. During this outage the estimated error standard deviation was 1 meter in both the east and north directions.

The experiment was repeated utilizing the tightly-coupled estimator (Fig. 8). During the outage the estimated error standard deviation was 2 meters in both the east and north directions. The tightly-coupled estimator has a similar offset from the CDGNSS position solution showing that there is an unknown source of error in the TRNS network causing the offset of the TRNS position solution.

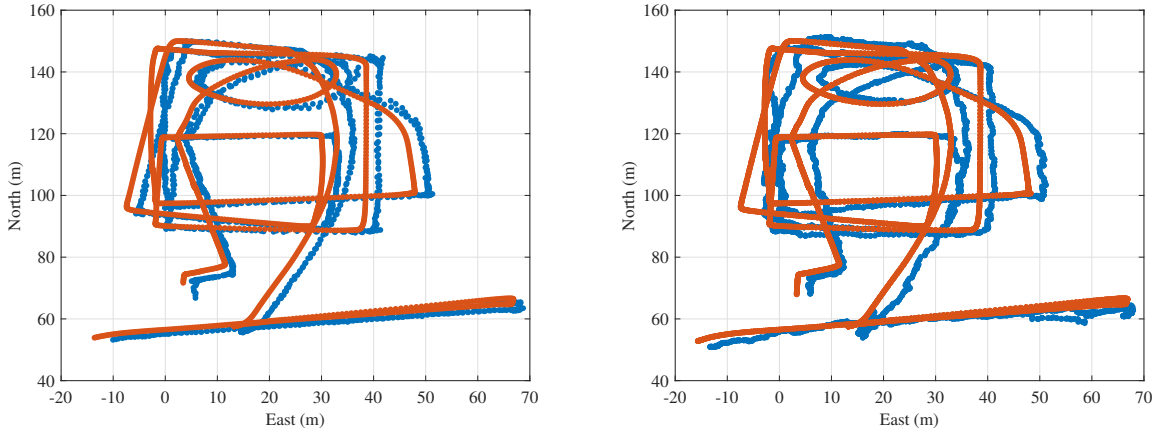

Fig. 8: Left: The blue is the loosely-coupled TRNS position solution during period of artificial GNSS outage. The orange is the CDGNSS position. Right: The blue is the tightly-coupled TRNS position solution during period of artificial GNSS outage. The orange is the CDGNSS position.

Intermittent Artificial GNSS Outages

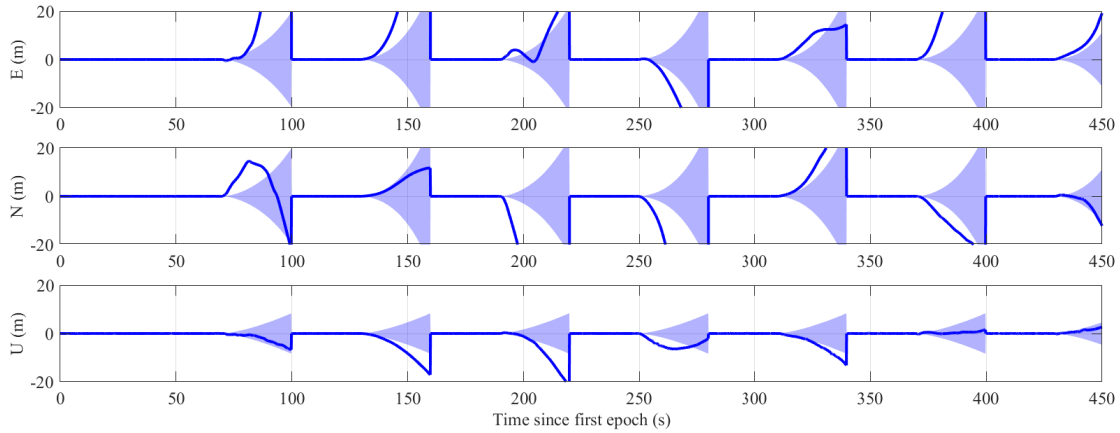

Fig. 9: Intermittent periods of artificial GNSS and TRNS outage. The solid blue shows the position errors in meters in the ENU frame due to the inertial sensor. The shaded region is the 1-σ uncertainty.

A UAM vehicle will likely only face interference or a loss of GNSS availability for a portion of the flight. A test of intermittent GNSS availability was preformed by artificially suppressing GNSS measurements from entering the estimator

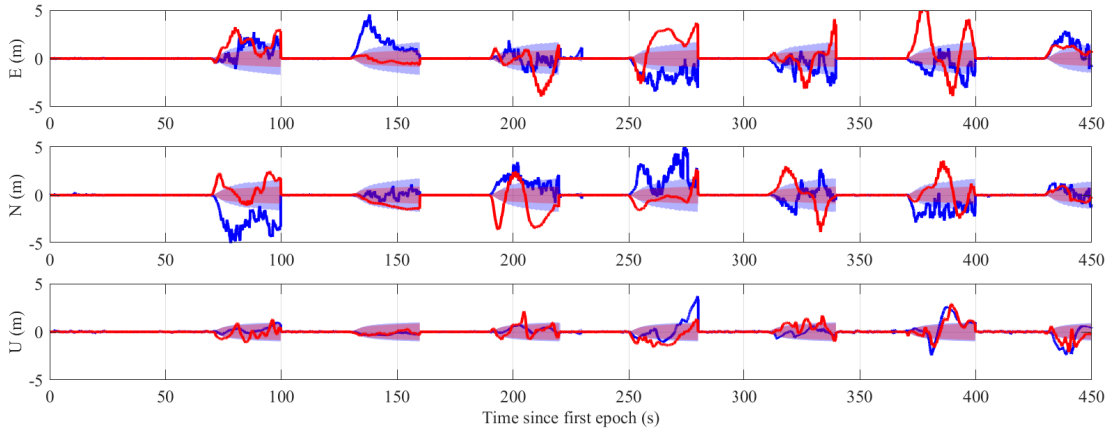

Fig. 10: Position errors in meters in the ENU frame during intermittent periods of artificial GNSS outages. The solid line is the error of the position estimate and the shaded region is the 1-σ uncertainty. The blue shows the tightly-coupled estimator while the red shows the loosely-coupled estimator.

for a duration of 30 seconds with a 60 second period. The estimator was first tested with a series of intermittent GNSS outages without the addition of the TRNS measurements (Fig. 9).

The error grows in the position during the outage is exponential. The exponential error growth is cause by drift in the consumer grade inertial sensor. During the short duration outage the 1-σ uncertainty grew to 28 meters in the east and north directions, and 8.4 meters in the Up direction. The maximum error during the test was found to be 166.7 meters, demonstrating the need for the addition of TRNS to constrain the error growth during GNSS outages.

The intermittent GNSS outages test was then preformed with the addition of TRNS measurements. The same interval was used so the tightly-coupled and loosely-coupled estimators could be directly compared to one another. For both tightly- and loosely-coupled estimators the addition of TRNS measurements served to constrain the error growth during GNSS outages (Fig. 10).

The loosely-coupled estimator 1-σ error uncertainty grew to 1 meter in each direction. In contrast, the tightly-coupled estimator 1-σ error uncertainty grew to 1.5 meter in the east and north directions while only growing to 1 meter in the Up direction. The tightly-coupled estimator had a larger uncertainty due to the unknown TRNS transmitter clock offsets. Both estimators had very similar behavior in the Up direction due to the poor vertical dilution of precision causing the position estimate in the Up direction to be heavily weighted by the pressure measurements.

CONCLUSION

TRNS provides a backup PNT source that can be utilized during GNSS outages to constrain the error growth of an inertial sensor. This paper demonstrates the first use of tightly-coupled CDGNSS, TRNS, and inertial sensing to provide a robust PVT solution on an aerial vehicle. An innovations-based measurement exclusion technique which mitigates the impact of TRNS multipath errors and pressure anomalies. A comparative analysis of loose and tight coupling on an aerial vehicle during simulated GNSS outages. It was found that during short duration GNSS outages the 1-σ position error in the east and north directions were 1 meter and 1.5 meters for the loosely- and tightly-coupled estimators respectively. Additional positioning systems will need to be added to provide overlapping layers to the DLN system in order to achieve decimeter accurate position during a GNSS outage. The results in this paper provide a first step in building such a system.

ACKNOWLEDGMENTS

Research support was provided by the U.S. Department of Transportation (USDOT) under the University Transportation Center (UTC) Program Grant 69A3552047138 (CARMEN), and by NextNav, an affiliate of the 6G@UT center within the Wireless Networking and Communications Group at The University of Texas at Austin.

REFERENCES

[1] Enge, P., "Local area augmentation of GPS for the precision approach of aircraft," *Proceedings of the IEEE*, Vol. 87, No. 1, 1999, pp. 111–132.

[2] Green, G. N. and Humphreys, T., "Position-Domain Integrity Analysis for Generalized Integer Aperture Bootstrapping," *IEEE Transactions on Aerospace and Electronic Systems*, Vol. 55, No. 2, 2018, pp. 734–746.

[3] Reid, T. G., Houts, S. E., Cammarata, R., Mills, G., Agarwal, S., Vora, A., and Pandey, G., "Localization Requirements for Autonomous Vehicles," *SAE International Journal of Connected and Automated Vehicles*, Vol. 2, No. 12-02-03-0012, 2019, pp. 173–190.

[4] Torens, C., Volkert, A., Becker, D., Gerbeth, D., Schalk, L., Garcia Crespillo, O., Zhu, C., Stelkens-Kobsch, T., Gehrke, T., Metz, I. C., et al., "HorizonUAM: Safety and Security Considerations for Urban Air Mobility," *AIAA Aviation 2021 Forum*, 2021, p. 3199.

[5] Yoder, J. E. and Humphreys, T. E., "Low-Cost Inertial Aiding for Deep-Urban Tightly-Coupled Multi-Antenna Precise GNSS," *Navigation, Journal of the Institute of Navigation*, 2022, To be published.

[6] Clements, Z., Yoder, J. E., and Humphreys, T. E., "Carrier-phase and IMU based GNSS Spoofing Detection for Ground Vehicles," *Proceedings of the ION International Technical Meeting*, Long Beach, CA, 2022.

[7] Rizos, C., Grejner-Brzezinska, D., Toth, C., Dempster, A., Li, Y., Politi, N., Barnes, J., and Sun, H., "A hybrid system for navigation in GPS-challenged environments: Case study," Vol. 4, 08 2009.

[8] Grejner-Brzezinska, D. A., Toth, C. K., Sun, H., Wang, X., and Rizos, C., "A Robust Solution to High-Accuracy Geolocation: Quadruple Integration of GPS, IMU, Pseudolite, and Terrestrial Laser Scanning," *IEEE Transactions on Instrumentation and Measurement*, Vol. 60, No. 11, 2011, pp. 3694–3708.

[9] Jiang, W., Li, Y., and Rizos, C., "Improved decentralized multi-sensor navigation system for airborne applications," *GPS Solutions*, Vol. 22, No. 78, 2018, https://doi.org/10.1007/s10291-018-0743-9.

[10] Jiang, W., Li, Y., Rizos, C., and Barnes, J., "Flight Evaluation of a Locata-augmented Multisensor Navigation System," *Journal of Applied Geodesy*, Vol. 7, 11 2013.

[11] Jiang, W., Li, Y., and Rizos, C., "Optimal Data Fusion Algorithm for Navigation Using Triple Integration of PPP-GNSS, INS, and Terrestrial Ranging System," *IEEE Sensors Journal*, Vol. 15, No. 10, 2015, pp. 5634–5644.

[12] Mohanty, A., Wu, A., Bhamidipati, S., and Gao, G., "Precise Relative Positioning via Tight-Coupling of GPS Carrier Phase and Multiple UWBs," *IEEE Robotics and Automation Letters*, 2022, pp. 1–1.

[13] Maaref, M., Khalife, J., and Kassas, Z. M., "Aerial Vehicle Protection Level Reduction by Fusing GNSS and Terrestrial Signals of Opportunity," *IEEE Transactions on Intelligent Transportation Systems*, Vol. 22, No. 9, 2021, pp. 5976–5993.

[14] Jia, M., Lee, H., Khalife, J., Kassas, Z. M., and Seo, J., "Ground Vehicle Navigation Integrity Monitoring for Multi-Constellation GNSS Fused with Cellular Signals of Opportunity," *2021 IEEE International Intelligent Transportation Systems Conference (ITSC)*, 2021, pp. 3978–3983.

[15] Brown, R. G. and Hwang, P. Y., *Introduction to Random Signals and Applied Kalman Filtering*, Wiley, 2012.

[16] Yoder, J. E., Iannucci, P. A., Narula, L., and Humphreys, T. E., "Multi-Antenna Vision-and-Inertial-Aided CDGNSS for Micro Aerial Vehicle Pose Estimation," *Proceedings of the ION GNSS+ Meeting*, Online, 2020, pp. 2281–2298.

[17] Humphreys, T. E., Murrian, M. J., and Narula, L., "Deep-Urban Unaided Precise Global Navigation Satellite System Vehicle Positioning," *IEEE Intelligent Transportation Systems Magazine*, Vol. 12, No. 3, 2020, pp. 109–122.

[18] Humphreys, T. E., Kor, R. X. T., and Iannucci, P. A., "Open-World Virtual Reality Headset Tracking," *Proceedings of the ION GNSS+ Meeting*, Online, 2020.

[19] Humphreys, T. E., Ledvina, B. M., Psiaki, M. L., and Kintner, Jr., P. M., "GNSS Receiver Implementation on a DSP: Status, Challenges, and Prospects," *Proceedings of the ION GNSS Meeting*, Institute of Navigation, Fort Worth, TX, 2006, pp. 2370–2382.

[20] Lightsey, E. G., Humphreys, T. E., Bhatti, J. A., Joplin, A. J., O'Hanlon, B. W., and Powell, S. P., "Demonstration of a Space Capable Miniature Dual Frequency GNSS Receiver," *Navigation*, Vol. 61, No. 1, Mar. 2014, pp. 53–64.

[21] Humphreys, T. E., Bhatti, J., Pany, T., Ledvina, B., and O'Hanlon, B., "Exploiting multicore technology in software-defined GNSS receivers," *Proceedings of the ION GNSS Meeting*, Institute of Navigation, Savannah, GA, 2009, pp. 326–338.

[22] Clements, Z., Iannucci, P. A., Humphreys, T. E., and Pany, T., "Optimized Bit-Packing for Bit-Wise Software-Defined GNSS Radio," *Proceedings of the ION GNSS+ Meeting*, St. Louis, MO, 2021.